


Non-polar GaN/AlGaN quantum-well polariton laser at room temperature

E. A. Amargianitakis^{1,2,*}, K. Tsagaraki², A. Kostopoulos,² G. Konstantinidis,² E. Delamadeleine,³
E. Monroy,³ and N. T. Pelekanos^{1,2}

¹*Department of Materials Science and Technology, University of Crete, P.O. Box 2208, 71003 Heraklion, Greece*

²*Microelectronics Research Group, Institute of Electronic Structure and Laser (IESL) Foundation for Research and Technology-Hellas (FORTH), P.O. Box 1385, 71110 Heraklion, Greece*

³*Université Grenoble Alpes (UGA), Commissariat à l'énergie atomique et aux énergies alternatives (CEA), Grenoble INP Institut d'ingénierie et de management, Institut de recherche interdisciplinaire de Grenoble (IRIG), Laboratoire PHotonique ELelectronique et Ingénierie QuantiqueS (PHELIQS), 17 avenue des Martyrs, 38000 Grenoble, France*

 (Received 16 June 2021; revised 27 August 2021; accepted 27 August 2021; published 24 September 2021)

We demonstrate room temperature (RT) polariton lasing in an all-dielectric microcavity containing non-polar III-nitride quantum wells (QWs) as active media. The microcavity is fabricated using the photo-electrochemical etching method, by which an optimally grown m -plane III-nitride active region is detached from the substrate in the form of a membrane, which is subsequently inserted between two $\text{SiO}_2/\text{Ta}_2\text{O}_5$ distributed Bragg reflectors, with 4 and 10 pairs for the top and bottom mirrors, respectively. The active region consists of 25 GaN/Al_{0.1}Ga_{0.9}N (5 nm/3 nm) QWs. The produced microcavities exhibit two closely spaced polarization-resolved lower polariton branches at RT, in line with the selection rules of the non-polar orientation, having a Rabi splitting of 62 and 72 meV in the $E \parallel a$ and $E \parallel c$ polarizations, respectively. In a positively detuned $3\lambda/2$ -thick microcavity, polariton lasing is observed at ambient conditions in the $E \parallel a$ polarization, with a threshold ~ 3 times lower than previous state of the art, despite the use of a relatively weak top reflector.

DOI: [10.1103/PhysRevB.104.125311](https://doi.org/10.1103/PhysRevB.104.125311)

I. INTRODUCTION

Exciton-polaritons are admixed exciton-photon quasiparticles that are formed inside semiconductor microcavities when the system operates under the strong coupling regime [1]. Due to their composite light-matter nature and bosonic character, above a certain density, exciton-polaritons are subjected to stimulated scattering, leading to Bose condensation at the $k = 0$ ground state of the lower polariton branch (LPB) [2]. The spontaneous emission of photons escaping the microcavity from this macroscopically coherent Bose condensate is the so-called polariton laser. Aside from their fundamental interest as inversionless sources of coherent and non-classical light, polariton lasers are attractive for their ability to operate at 100 times lower threshold currents than conventional laser diodes [3]. First realizations of polariton lasers were based on GaAs [4–6] and CdTe [7] active layers, but the strong coupling conditions were preserved only at cryogenic temperatures due to the weak exciton binding energies in these systems. For proper operation at ambient temperature, wide band gap semiconductors are the system of choice due to the increased exciton binding energies, which are comparable or higher than $k_B T$ [8]. Several GaN polariton lasers operating at room temperature (RT) under optical excitation have been reported, using in standard vertical emission planar geometries bulk GaN [9], GaN quantum wells (QWs) [10], or even GaN nanowires [11] as active media. Electrical injection has been

also demonstrated using bulk GaN as active material; however, this was accomplished in a non-standard edge-emitting in-plane microcavity [12].

A few years ago, our group demonstrated a RT GaN polariton laser [13] exhibiting the highest Rabi splitting value of 64 meV and the lowest polariton lasing threshold under quasicontinuous excitation ($P_{\text{thr}} = 4.5 \text{ W/cm}^2$) compared with previous reports using bulk or QW structures. The major advantage in that demonstration was the fabrication method. Unlike earlier realizations, where the GaN-based active region was grown either on heavily mismatched substrates such as silicon [14] or on monolithic AlInN/GaN distributed Bragg reflectors (DBRs) with an excessive number of periods [15], our polariton laser was fabricated using the photo-electrochemical (PEC) etching method [16–20]. The PEC method allows for the detachment from the substrate of an optimally grown active region in the form of an atomically smooth membrane [21], which is subsequently incorporated inside an all-dielectric microcavity. Recently, an even higher Rabi splitting of 71 meV at RT was achieved with the PEC method, using an improved microcavity design containing GaN/AlGaN QWs in the entire range of the active region and an only-4-pair DBR as a top mirror [22].

Most of the available literature on GaN microcavities and polariton lasers is based on polar material [9–22], grown along the c crystallographic axis, in accordance with the generally preferred orientation of III-nitrides. It is well known, however, that polar III-nitride heterostructures suffer from giant piezoelectric and spontaneous polarization-induced electric fields [23–26], which tend to weaken the QW optical

*amargian@materials.uoc.gr

transitions via the quantum-confined Stark effect. To alleviate this problem, several approaches have been examined in the past. The most typical one consists of using narrow polar QWs (thickness < 3 nm) [24,25], which limit the Stark effect and have enabled the observation of strong coupling and polariton lasing phenomena in polar GaN QW microcavities [10,13]. Another interesting possibility is the polarization-matching in quaternary InAlGaN/GaN polar heterostructures [27–29]. However, perhaps the most promising method of all consists of using *m*- or *a*-plane non-polar QWs, which are inherently free of internal electric fields [30–32].

Despite the enhanced strong coupling characteristics that can be expected in polarization-free orientations, only a few non-polar QW microcavities have been demonstrated so far. Authors of early reports on non-polar microcavities, using monolithic nitride-based bottom DBRs with a moderately high degree of disorder, have shown strong coupling at RT [33], polarization-dependent strong coupling effects [34], and polariton lasing at 50 K, albeit with relatively large thresholds [35]. Strong coupling effects and polariton trapping at RT were also observed in non-polar GaN/AlGaIn microcavities with air-gap DBRs [36,37]. In this paper, we have adapted the PEC-etching approach to the *m*-plane configuration to fabricate leading-edge non-polar GaN QW microcavities with oxide DBRs, based on high optical quality GaN/AlGaIn QWs, epitaxially grown on commercial *m*-plane GaN bulk substrates. In our primary structures, we have observed two closely spaced polarization-resolved LPBs as well as polariton lasing at RT, with a lasing threshold ~ 3 times lower than the previous record low value [13].

II. NON-POLAR GaN/AlGaIn QWs

To ensure an active region of superior optical quality, the non-polar GaN/AlGaIn QWs were grown by plasma-assisted molecular beam epitaxy on freestanding 320- μm -thick nominally undoped *m*-plane GaN substrates from Suzhou Nanowin Ltd. The growth conditions of the active region are described elsewhere [38,39]. In contrast to hetero-epitaxial growth of non-polar GaN on foreign substrates, such as Al_2O_3 [31,40], $\gamma\text{-LiAlO}_2$ [30], 4*H*-SiC or 6*H*-SiC [41], or ZnO [42], the use of freestanding *m*-plane GaN substrates leads to active regions grown with zero thermal strain and a dislocation density $< 10^6 \text{ cm}^{-2}$. In this paper, a stack of 25 GaN/Al_{0.1}Ga_{0.9}N (5 nm/3 nm) QWs forms the $3\lambda_o/2n$ -thick active region, with λ_o being the QW emission wavelength and n the average refractive index of the cavity. The main reason for using 5-nm-thick QWs was to minimize the inhomogeneous broadening occurring in thinner nitride QWs due to interface roughness and compositional fluctuations in the AlGaIn barriers [31,32]. The active region was grown on top of a 25-nm-thick InGaIn sacrificial layer with a targeted indium composition $\sim 12\text{--}14\%$. The well-known problem of low In incorporation in non-polar growth [43] was addressed in our case by growing several identical samples at decreasing substrate temperature, thus attaining a high enough indium content in the sacrificial layer to allow PEC etching with a continuous wave (cw) laser diode emitting at 405 nm.

The exciton levels of the as-grown multi-QW samples have been characterized by polarization-resolved photoluminescence

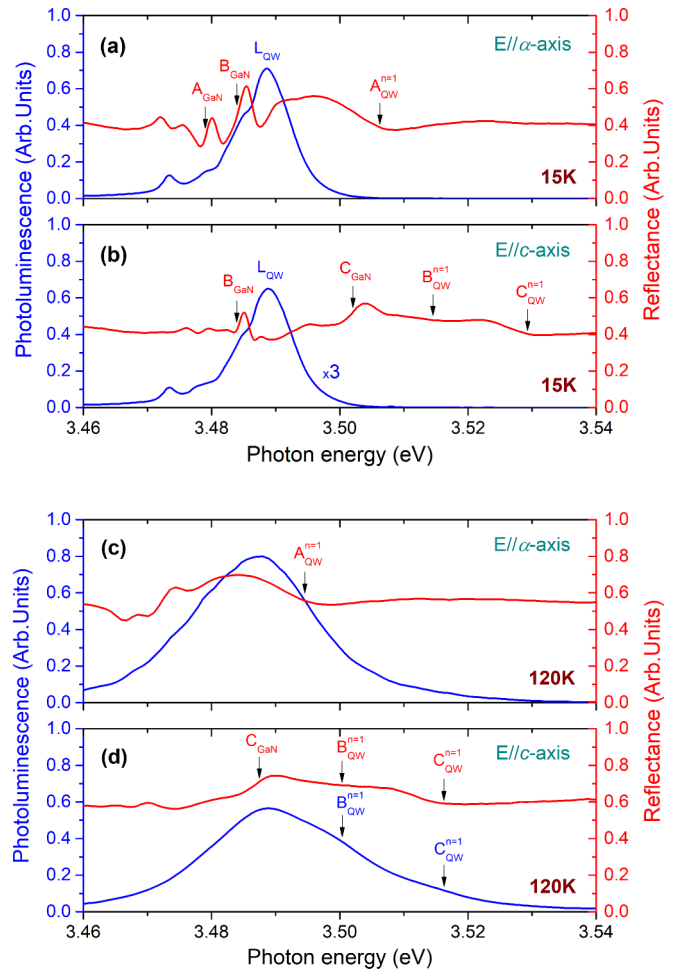


FIG. 1. Polarization-resolved photoluminescence (PL) and reflectivity (RFL) spectra from the as-grown non-polar multi-quantum-well (QW) structure, recorded at 15 K in the (a) $E \parallel a$ polarization and (b) $E \parallel c$ polarization. (c) and (d) The same PL and RFL spectra, recorded at 120 K.

and reflectivity (RFL) spectroscopy as a function of temperature, using as excitation a He-Cd cw laser at 325 nm and a broadband Xenon 150 W lamp, respectively. In Fig. 1, we present the PL and RFL spectra of the as-grown GaN/AlGaIn QWs, obtained at 15 and 120 K in the two orthogonal polarizations ($E \parallel a$ and $E \parallel c$) analyzed by a calcite Glan-Taylor prism and a ultraviolet $\lambda/2$ waveplate. The polarized RFL intensities were normalized to an arbitrary unit to compare the relative oscillator strengths in the two polarizations. The full set of polarized RFL spectra with varying polarization angle is given in Fig. S1 in the Supplemental Material [44]. In general, the non-polar QW samples are characterized by enhanced PL intensities compared with their polar counterparts grown during the same epitaxial run, while the RFL spectra exhibit pronounced exciton features, demonstrating the marked exciton-photon interaction of non-polar excitons as well as the high optical quality of the *m*-plane QWs.

In the $E \parallel a$ -polarized RFL spectrum of Fig. 1(a), we distinguish at 15 K the bulk A_{GaN} and B_{GaN} excitons located at 3.479 and 3.484 eV, respectively. These energy values agree

with previous studies on unstrained bulk m - or a -plane GaN [45–48], where both the A_{GaN} and B_{GaN} exciton states were found to be allowed in the $E \parallel a$ polarization. In the same polarization, a relatively broader QW-exciton feature is well resolved at 3.506 eV, which we attribute to the $n = 1$ A_{QW} exciton state based on its position and polarization dependence. The full width at half maximum (FWHM) linewidth of the A_{QW} exciton is ~ 11 meV, within the lowest exciton FWHM linewidth values reported in the literature for single non-polar QW grown on bulk GaN [49]. In the same spectrum, a weaker feature is also visible at 3.529 eV that we attribute to the “forbidden” C_{QW} exciton.

In the cross-polarized RFL spectrum of Fig. 1(b), the B_{GaN} and C_{GaN} bulk excitons are clearly visible at 3.484 and 3.502 eV, respectively, while the A_{GaN} exciton almost disappeared, in accordance to the polarization selection rules for non-polar GaN [46,47]. According to the same rules, the C_{GaN} line is usually observed in both polarizations, with the $E \parallel a$ component being much weaker. In our case, however, it is difficult to distinguish the C_{GaN} exciton in the $E \parallel a$ polarization due to the near coincidence with the $n = 1$ A_{QW} exciton at 3.506 eV. In the $E \parallel c$ polarization, the allowed QW transitions are the B_{QW} line at 3.514 eV and the C_{QW} one at 3.529 eV, as shown in Fig. 1(b). This assignment is further supported by the observation of bumplike PL emission from the B_{QW} and C_{QW} states at higher temperatures, as indicated in the PL spectrum in Fig. 1(d).

The above results strongly suggest that the polarization selection rules in our GaN/AlGaIn QWs are such that the A_{QW} line is $E \parallel a$ polarized, while the B_{QW} and C_{QW} lines are $E \parallel c$ polarized. As previously discussed in the literature [34,35], the exciton selection rules and relative oscillator strengths in non-polar GaN/AlGaIn QWs depend strongly on valence band mixing and strain effects induced by the lattice mismatch between GaN and AlGaIn. In our case, the results are in qualitative agreement with the $\mathbf{k}\cdot\mathbf{p}$ estimates of Ref. [34] for GaN/AlGaIn QWs with Al content in the 5–10% range. In the referred work, the Al content was assumed to control the strain of the GaN layers, which strictly speaking was not the case in our as-grown samples, where the GaN layers were lattice-matched to the substrate. This is the case, however, in our freestanding GaN/Al_{0.1}Ga_{0.9}N QW membranes, where the GaN QW layers acquire a compressive strain due to the presence of the AlGaIn layers, which is proportional to the Al composition.

Regarding PL, the secondary emission spectrum at 15 K derives mainly from localized A_{QW} -exciton states, denoted by L_{QW} , as evidenced by the fact that the main QW PL peak does not vary in energy in the two polarizations, while the emission is maintained strongly polarized along $E \parallel a$ [50]. Please note that the PL spectrum in Fig. 1(b) is multiplied by a factor of 3 for better visibility. With increasing temperature, a thermally induced delocalization process sets in, gradually reducing the Stokes shift between the QW emission peak and the free QW exciton features observed in RFL. This effect is evident in the $E \parallel a$ -polarized PL/RFL spectra of Fig. 1(c), where the PL peak at 120 K has acquired a significant overlap with the respective A_{QW} feature in RFL. The fact that the delocalization process is completed in the 100–120 K range is corroborated by the S-like behavior of the QW emission

energy with temperature, depicted in Fig. S2 in the Supplemental Material [44], as well as by the temperature-dependent exciton decay times shown in Fig. S3(a) in the Supplemental Material [44], which clearly suggest a change of regime at ~ 100 K. The analysis presented in Fig. S3 in the Supplemental Material [44] further confirms the high optical quality of the as-grown non-polar QWs. Particularly, the PL intensity drops only by a factor of 24 between 20 and 300 K, while the PL decay time at RT of non-radiative origin is quite long ~ 400 ps. The latter is significantly higher than previously reported values for single non-polar QWs, including for QWs grown on bulk GaN [49], and reflects the reduced non-radiative channels in our structure. The above characteristics make these optimally grown QWs ideal for polaritonic devices.

III. MICROCAVITY FABRICATION

Next, we turn our attention to the fabrication of the polariton devices. As a first step, the surface of the as-grown sample was patterned into ~ 1 - μm -deep square mesas with areas from $45 \times 45 \mu\text{m}^2$ to $155 \times 155 \mu\text{m}^2$, by combining photolithography and reactive ion etching. Then the sample was attached to a PEC cell, where an area of 0.78 mm^2 got in contact with a dilute KOH (4×10^{-4} M) solution and became illuminated for ~ 45 min by 4.5 mW of a cw 405 nm laser diode. These conditions are sufficient for the complete and smooth lateral etching of the InGaIn sacrificial layer [21] and the release of many ultrathin membranes. As illustrated in Fig. 2(b), the successful PEC etching of the InGaIn layer is visible by the distinct color change of the etched mesas with respect to the background. The released membranes were then transferred one by one on other substrates of choice using a probe tip [51]. For instance, by transferring the sub-micron-thick membranes on sapphire, it is possible to perform microtransmittance (μ - T) measurements and directly deduce the optical density (OD) and oscillator strength of the exciton states involved in the polariton formation [22,51].

In Fig. 2(c), we present the deduced OD spectra at RT in the $E \parallel a$ and $E \parallel c$ polarizations from a 200-nm-thick membrane containing 25 non-polar GaN/AlGaIn QWs. We distinguish two pronounced exciton resonances in the two polarizations of approximately the same strength separated by ~ 12 meV. In agreement with the polarization selection rules determined for the as-grown samples in the previous section, we attribute the $E \parallel a$ -excitonic resonance to A_{QW} excitons and the $E \parallel c$ resonance to a combined contribution from the B_{QW} and C_{QW} excitons. Dividing by the number of QWs, we determined the OD per QW at the peak, varying between 4.4 and 4.9% in the two polarizations. Moreover, the integration of the OD(E) curves yields an exciton oscillator strength of $4 \times 10^{13} \text{ cm}^{-2}$ in the $E \parallel a$ polarization and of $5.6 \times 10^{13} \text{ cm}^{-2}$ in the $E \parallel c$ polarization.

The above values confirm the enhanced oscillator strengths of the non-polar orientations, as they are already higher or comparable with those of much thinner polar QWs, such as 2.7-nm-thick polar GaN/Al_{0.07}Ga_{0.93}N QWs, for which an OD per QW of 3.5% and an exciton oscillator strength of $4.5 \times 10^{13} \text{ cm}^{-2}$ have been reported [22]. In addition to the above “dichroic” behavior, the m -plane GaN/AlGaIn QWs are

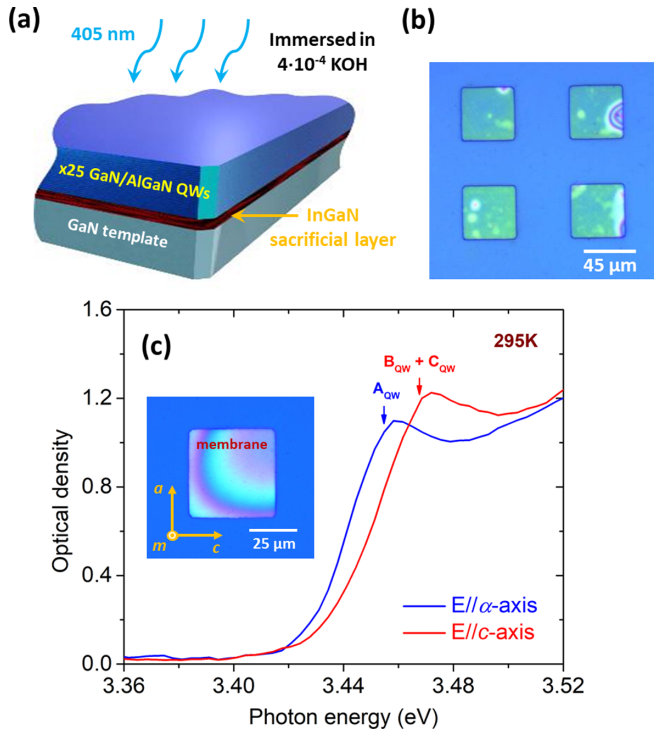


FIG. 2. (a) Schematic of the band-gap-selective photoelectrochemical (PEC) etching of an InGaN layer for the membrane separation, (b) optical image of a PEC-etched region, and (c) optical density of an m -plane membrane with embedded 25 GaN/Al_{0.1}Ga_{0.9}N quantum wells (QWs) as extracted from room temperature (RT) μ -transmittance measurements acquired in the $E \parallel a$ - and $E \parallel c$ -axis polarizations of the electric field. The inset shows a freestanding membrane, transferred on a 10-pair bottom-distributed Bragg reflector (DBR)/Si substrate for microcavity fabrication.

also expected to exhibit significant birefringence in the two polarizations due to the inherent crystal anisotropy. For m -plane GaN, the birefringence is positive, i.e., the extraordinary ($E \parallel c$) index of refraction n_e exceeds the ordinary ($E \parallel a$) index of refraction n_o by about 1.5–2% in the transparent spectral region and by <1% as we approach the gap [52,53]. Both dichroic and birefringence effects are important in accounting for the anisotropic polariton dispersions, discussed next. To investigate the strong coupling regime, the 200-nm-thick membranes containing 25 non-polar GaN/AlGaIn QWs were transferred on a 10-pair SiO₂/Ta₂O₅ bottom DBR pre-deposited on a Si substrate, as shown in the inset of Fig. 2(c). To complete the microcavity, a top DBR was either deposited [22] or directly transferred [54] on top of the GaN/AlGaIn membrane. In this paper, we report on all-dielectric non-polar GaN/AlGaIn microcavities fabricated by electron-gun deposition of a 4-pair SiO₂/Ta₂O₅ top DBR. A schematic of a complete microcavity is given in Fig. 3.

IV. ANISOTROPIC POLARITON EMISSION

The pronounced polaritonic character of the non-polar microcavities was established by k -space imaging or angle-resolved micro-PL (μ -PL) measurements at RT. The micro-

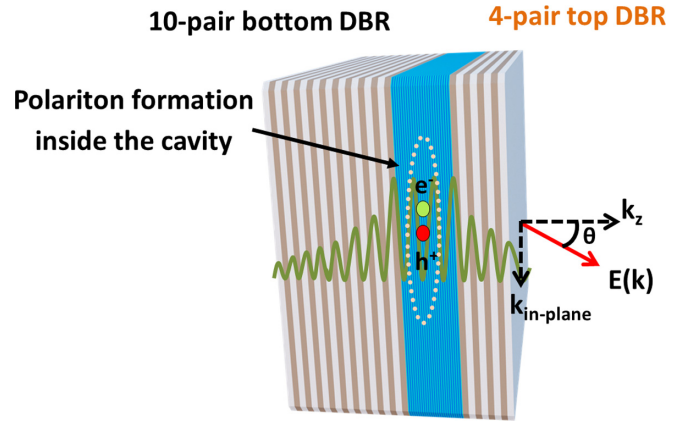


FIG. 3. Schematic illustration of a $3\lambda/2$ non-polar microcavity, consisting of 25 m -plane GaN/AlGaIn quantum wells (QWs) sandwiched between a 4-pair (top) and a 10-pair (bottom) SiO₂/Ta₂O₅ distributed Bragg reflector (DBR). Such a microcavity can operate in the strong coupling regime and exhibit room temperature (RT) polariton lasing.

cavity sample was excited at normal incidence by a cw 325 nm laser beam, focused down to a 9 μ m spot using an aspherical lens with numerical aperture (NA) = 0.63. The μ -PL signal was collected through the same optical path using a beam splitter and a final collection lens. For angle-dependent measurements, an additional lens was positioned at a certain position before the final lens, imaging the Fourier plane of the aspheric lens into the spectrometer. Thus, the polariton emission was recorded simultaneously for a range of angles between $\pm 39^\circ$, determined by the NA of the optical path, tracing directly the polariton dispersions of the system.

Figure 4 depicts polarization-resolved k -space images from a typical non-polar microcavity at 295 K, exhibiting two distinct LPBs in the two polarizations. Like most polar nitride polariton devices [9,10,13], no upper polariton branches (UPBs) are visible here, most likely due to the rapid decay of UPBs to higher energy exciton and continuum states. Comparing the two LPBs, the one in the extraordinary $E \parallel c$ configuration (LPB_e) is much more dispersive than that in the ordinary $E \parallel a$ configuration (LPB_o). In addition, LPB_e exhibits between the two the lowest energy at $k = 0$ and flattens out to a higher energy level at high k . This implies that the two LPBs intercross at some specific angle, an unusual feature for a semiconductor microcavity.

To explain the above LPB dispersions, one must consider both the birefringence and the anisotropic exciton oscillator strength in the two polarizations. Specifically, as pointed out earlier, LPB_o arises due to the strong coupling of the A_{QW} excitons with the ordinary cavity mode C_o [dotted curve in Fig. 4(a)]. Likewise, LPB_e is formed by the interaction between the B_{QW} + C_{QW} excitons and the extraordinary cavity mode C_e [dotted curve in Fig. 4(b)]. In Fig. 4, the position of the A_{QW} exciton is taken at 360.4 nm (3.440 eV) and that for the B_{QW} + C_{QW} exciton at 359.4 nm (3.450 eV). Considering the positive birefringence effect in GaN, with $n_e > n_o$, the C_e cavity mode is expected at a longer wavelength with respect to C_o. This, as we shall see below, leads to the unusual coexistence in our microcavity of a more “photonic,”

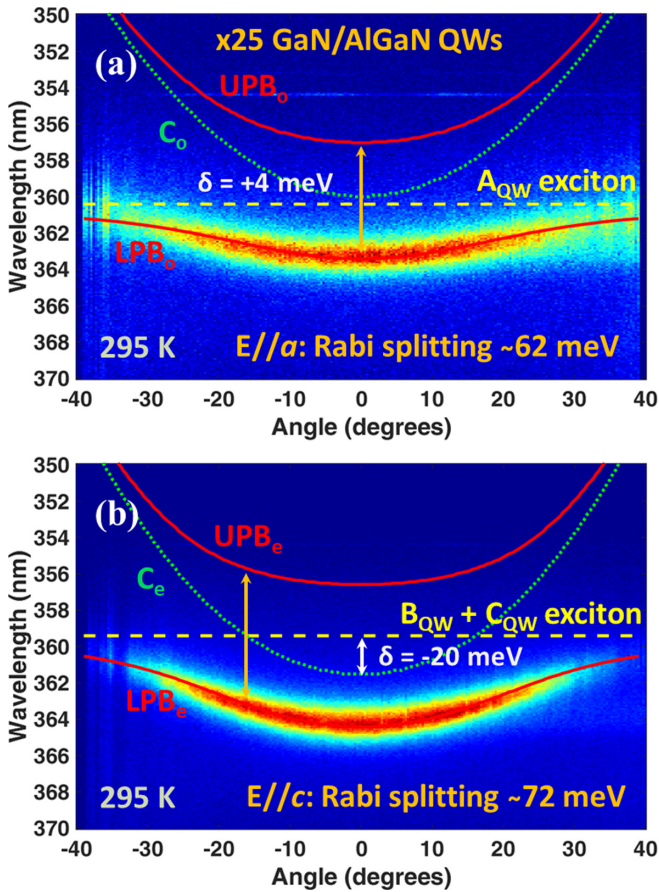


FIG. 4. Polarization-resolved k -space imaging of the μ -photoluminescence (PL) emitted at room temperature (RT) by a non-polar $3\lambda_0/2n$ -microcavity with 4- and 10-pair distributed Bragg reflector (DBR) mirrors, exhibiting a Rabi splitting of (a) 62 meV and (b) 72 meV in the $E \parallel a$ and $E \parallel c$ polarization, respectively. The ordinary (C_o) and extraordinary (C_e) cavity modes (green dotted lines), the A_{QW} and $B_{QW} + C_{QW}$ exciton levels in the two polarizations (yellow dashed lines), as well as the simulated lower- and upper-polariton branches (red solid curves) are also shown.

negatively detuned LPB_e along with a more “excitonic,” positively detuned LPB_o . The different detuning along with the 40% higher oscillator strength for the combined $B_{QW} + C_{QW}$ exciton peak explains how, at $k = 0$, the LPB_e is at longer wavelengths than LPB_o . The values of the LPBs at zero angle are 363.4 nm (3.411 eV) for LPB_o and 364.1 nm (3.402 eV) for LPB_e .

To best fit the LPB dispersions, we proceed as follows. We first determine the thicknesses of the oxide layers, by fitting with a transfer matrix model (TMM) [55] the RFL spectra of the “witness” top DBR/Si, grown during the same deposition run, the bottom DBR/Si, and the $\lambda/2$ resonator formed by the deposition of the top DBR on a bottom DBR/Si. Moreover, the thickness of the GaN-based membrane as well as the difference $\Delta n = n_e - n_o$ are extracted by fitting the Fabry-Perot oscillations in the transparent region of polarization-resolved μ - T spectra. This procedure allows us to estimate with precision, based on TMM, the cavity

modes in the two polarizations, with the $k = 0$ C_o position being at 360 nm (3.444 eV) and the C_e position at 361.6 nm (3.430 eV). This cavity mode difference corresponds to a $\Delta n = 0.025$, which is a reasonable value based on the literature [52,53] for the spectral region near the excitonic gaps. Accordingly, the values of detuning for the two polarizations are +4 meV for $E \parallel a$ and -20 meV for $E \parallel c$. By knowing the cavity mode and exciton level in each polarization, it is then possible to sensitively fit the LPB dispersions in Fig. 4 with the Hamiltonian model, using the respective coupling constants as adjustable parameters. The coupling constants that best reproduce the LPB dispersions are 31.4 meV for $E \parallel a$ and 36.7 meV for $E \parallel c$. The somewhat higher coupling constant for the $E \parallel c$ configuration is justified by the higher oscillator strength of the $B_{QW} + C_{QW}$ exciton peak. Knowing the coupling constants in the two polarizations, we can then estimate the respective Rabi splittings by the energy difference at the anticrossing between the calculated LPB and UPB dispersions, which amount to 62 meV for $E \parallel a$ and 72 meV for $E \parallel c$, respectively. To our knowledge, these values set the state of the art for non-polar nitride QW microcavities [33–35] and demonstrate the high quality and optimum design of our structures.

V. POLARITON LASING AT RT

The successful observation of robust RT polaritons in the non-polar microcavities has prompted the study of polariton lasing in this particularly intriguing system. Toward this end, we excited the sample with a quasicontinuous 266 nm frequency-quadrupled Nd:YAG pulsed laser (7.58 kHz repetition rate and 0.51 ns pulse width) at normal incidence, using the same k -space imaging setup as previously described. The alignment of the k -space setup was optimized at the emission wavelength of the GaN QWs (≈ 360 nm). Due to the elliptical shape of the laser beam and the chromaticity of the optics, the excitation spot size in this experiment was $10 \times 60 \mu\text{m}^2$. Figure 5 shows the k -space images of the LPB_o emission ($E \parallel a$ polarization) at RT, with increasing excitation power from below to above a threshold power density of $P_{\text{thr}} = 1.75 \text{ W/cm}^2$, obtained by linear extrapolation of the intensity vs power curve in Fig. 5(f). At low powers ($0.34 \cdot P_{\text{thr}}$), a dispersion curve is observed in Fig. 5(a), very similar to Fig. 4(a) for cw excitation, corresponding to an LPB created by the interaction of A_{QW} excitons with the ordinary cavity mode, as fitted using the Hamiltonian model. With power increasing to 0.47 and $0.74 \cdot P_{\text{thr}}$ [Figs. 5(b) and 5(c)], the LPB_o emission concentrates to lower angles, becomes spectrally narrower, and blueshifts in energy with respect to lower excitation, as a manifestation of polariton-polariton interaction [56,57]. The onset of polariton lasing is marked by an abrupt non-linear increase of the spectrally integrated $k = 0$ μ -PL intensity with a concomitant collapse of linewidth down to ≈ 2 meV, as depicted in Fig. 5(f).

A strong indication that the system remains in the strong coupling regime above threshold is that the polariton laser line appears at distinctly longer wavelengths than the C_o cavity mode and the A_{QW} exciton for all powers larger than P_{thr} , as shown for instance in the k -space image of Fig. 5(d) for $1.27 \cdot P_{\text{thr}}$. The observed P_{thr} is ~ 3 times lower than the

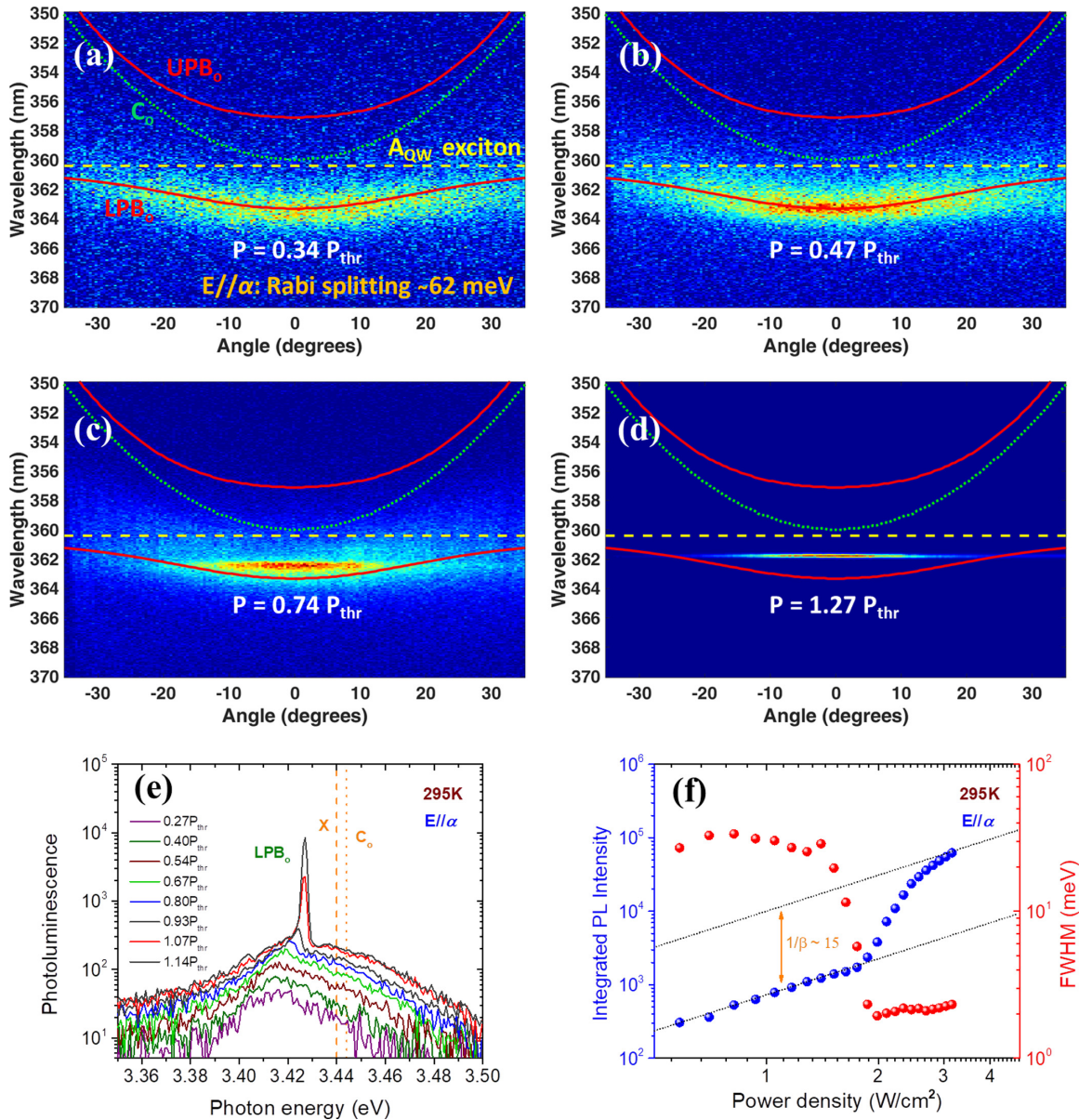


FIG. 5. (a)–(d) Sequence of room temperature (RT) k-space μ -photoluminescence (PL) images obtained from the non-polar $3\lambda_o/2n$ -microcavity in the $E \parallel a$ polarization, with increasing pumping power from a quasicontinuous pulsed 266 nm laser, below and above a power threshold of $P_{\text{thr}} = 1.75 \text{ W}/\text{cm}^2$. (e) μ -PL spectra at $k = 0$ as a function of pumping power. (f) Nonlinear increase of the spectrally integrated $k = 0$ μ -PL intensity and corresponding line narrowing as we cross the polariton lasing threshold.

previous state-of-the-art value reported for a polar GaN QW microcavity [13] and >10 times lower than the threshold power density for polariton lasing at 50 K in a non-polar QW microcavity [35]. It is important to mention that the same excitation source was used in all these comparative works. The comparison is even more impressive considering that the top DBR mirror consists of only four periods in our case, further illustrating the large potential of all-dielectric non-polar microcavities as efficient polariton lasers.

An estimate of the carrier density at threshold can be obtained from the blueshift (ΔE) of the LPB line, when increasing the pump power up to the threshold value. From the $k = 0$ μ -PL spectra of Fig. 5(e), we deduce that the blueshift experienced by LPB_o polaritons is $\Delta E = 8 \text{ meV}$. Using the

relation $\Delta E = 6|X_0|^2 E_B a_B^2 N_{2D}$ [56,57], where $|X_0|^2 (\approx 0.53)$ is the exciton fraction of the LPB_o polaritons at $k = 0$, $E_B (\approx 40 \text{ meV})$ is the exciton binding energy, and $a_B (\approx 2.8 \text{ nm})$ is the exciton Bohr radius, we can estimate the exciton density at threshold as being equal to $N_{2D} = 8 \times 10^{11} \text{ cm}^{-2}$. It should be noted that the above relation neglects exciton-saturation effects, which also tend to blueshift LPBs, and thus provides only an upper estimate of the exciton density at threshold. Anyway, the estimated N_{2D} is still significantly lower than the exciton saturation density in nitride QWs of $\approx 2 \times 10^{12} \text{ cm}^{-2}$ [58], further asserting that we are in the strong coupling regime. In Fig. 5(f), the integrated intensity vs pump power exhibits the expected S-like behavior corresponding to a β -factor of $\sim \frac{1}{15}$. It should be noted that, in the context of a

polariton laser, the β -factor represents the fraction of polaritons spontaneously emitted in the mode undergoing stimulated scattering [9]. The relatively large β -factor value observed here is possibly due to the reduced “polariton volume” in our case. For instance, if we compare the all-dielectric microcavity of this paper with that of a microcavity having only one dielectric DBR on top and exhibiting a much smaller β -factor of $\frac{1}{7000}$ [9], the polariton confinement along the z direction is significantly stronger in our case. Likewise, if we compare with a very similar negatively detuned polar QW microcavity, having dielectric DBRs on both sides and a β -factor of $\frac{1}{50}$ [13], again, the polariton volume is expected to be smaller in our positively detuned non-polar microcavity due to the significant in-plane localization of the polariton condensate during polariton lasing. This is manifested in the relatively large angle spread of the polariton laser emission seen in Fig. 5(d) that we can attribute to spatial confinement of the polariton condensate in photonic disorder [59]. The observed angle spread of $\pm 8^\circ$ corresponds to a localization radius for the polariton condensate of $\sim 0.4 \mu\text{m}$, a reasonable value for positively detuned polaritons in a nitride microcavity [60].

Interestingly, in the $E \parallel c$ polarization, the LPB_e polaritons exhibit no polariton lasing, at least in the power range used in Fig. 5. This result is presently not fully understood and deserves further investigation. The main parameters determining the polariton lasing threshold in a semiconductor microcavity are the polariton lifetime inside the $k = 0$ trap, the polariton relaxation dynamics down the LPB dispersion, and—for high temperatures—the thermal escape of polaritons from the trap to the exciton reservoir [60]. For a constant temperature, the latter process should be particularly sensitive to the energy depth of the polariton trap with respect to the exciton reservoir. By inspection of Fig. 4, however, the trap is deeper for LPB_e polaritons ($\approx 50 \text{ meV}$) than LPB_o polaritons ($\approx 30 \text{ meV}$), implying that the non-observation of polariton lasing in the LPB_e dispersion cannot be associated with the thermal escape process. On the other hand, based on the anisotropic polariton dispersions in Fig. 4, one can qualitatively argue that the positively detuned LPB_o polaritons ($\delta = +4 \text{ meV}$) have longer decay time at $k = 0$ and shorter relaxation times down the polariton dispersion than the negatively detuned LPB_e polaritons ($\delta = -20 \text{ meV}$). Specifically, the LPB_o polariton lifetime at $k = 0$ is estimated to be 0.4 ps using $|X_0|^2 \approx 0.53$, a cavity time of 0.19 ps , and an exciton decay time at RT of 384 ps , while that for LPB_e polaritons with $|X_0|^2 \approx 0.37$ becomes 0.3 ps . Likewise, the polariton effective masses along the “more excitonic” LPB_o dispersion

are considerably larger than LPB_e , enhancing the scattering probability and shortening the relaxation time from the exciton reservoir to the polariton trap. Both effects favor the accumulation of polaritons in the LPB_o polariton trap compared with LPB_e , leading to the macroscopic condensation and the observation of polariton lasing solely in the $E \parallel a$ configuration. Evidence for a weaker LPB_e population can be found in the much smaller blueshift ($\approx 4 \text{ meV}$) of the LPB_e line than the LPB_o as we increase the pump power up to the threshold value. Assuming the same exciton parameters for the two LPBs and a $|X_0|^2 \approx 0.37$ for the LPB_e polaritons, we find that the LPB_e population is $\sim 70\%$ that of the LPB_o polaritons, in agreement with the qualitative argument presented above. Clearly, further studies are necessary to elucidate this important point.

VI. CONCLUSIONS

In summary, RT polariton lasing is demonstrated in an all-dielectric non-polar III-nitride QW microcavity fabricated by means of the PEC etching method. The $3\lambda/2$ microcavity consists of 25 polarization-free m -plane GaN/ $\text{Al}_{0.1}\text{Ga}_{0.9}\text{N}$ active QWs sandwiched between two $\text{SiO}_2/\text{Ta}_2\text{O}_5$ DBRs and presents two distinct polarization-orthogonal LPBs, with a RT Rabi splitting of 62 and 72 meV in the $E \parallel a$ and $E \parallel c$ polarizations, respectively. Despite the use of a relatively weak top reflector, polariton lasing is observed in the positively detuned LPB along the $E \parallel a$ polarization, with an ultralow threshold of 1.75 W/cm^2 at ambient conditions, which is ~ 3 times lower than the previous state of the art among reported nitride-based thin film microcavities. These results are very encouraging for further development of highly efficient non-polar nitride polariton devices.

ACKNOWLEDGMENTS

This paper was supported by the Stavros Niarchos Foundation within the framework of the project Advancing Young Researchers’ Human Capital in Cutting Edge Technologies in the Preservation of Cultural Heritage and the Tackling of Societal Challenges, and by Greece and the European Union (European Social Fund) through the Programme Human Resources Development, Education and Lifelong Learning 2014–2020 in the context of the project Nanophotonic Semiconductor Sources of Single and Entangled Photons (MIS 5048530). Financial support from the French ANR project UVLASE (No. ANR-18-CE24-0014) is also acknowledged.

- [1] C. Weisbuch, M. Nishioka, A. Ishikawa, and Y. Arakawa, Observation of the Coupled Exciton-Photon Mode Splitting in a Semiconductor Quantum Microcavity, *Phys. Rev. Lett.* **69**, 3314 (1992).
- [2] A. İmamoğlu, R. J. Ram, S. Pau, and Y. Yamamoto, Nonequilibrium condensates and lasers without inversion: Exciton-polariton lasers, *Phys. Rev. A* **53**, 4250 (1996).
- [3] H. Deng, G. Weihs, D. Snoke, J. Bloch, and Y. Yamamoto, Polariton lasing vs. photon lasing in a semiconductor microcavity, *Proc. Natl. Acad. Sci.* **100**, 15318 (2003).

- [4] P. Bhattacharya, B. Xiao, A. Das, S. Bhowmick, and J. Heo, Solid State Electrically Injected Exciton-Polariton Laser, *Phys. Rev. Lett.* **110**, 206403 (2013).
- [5] C. Schneider, A. Rahimi-Iman, N. Y. Kim, J. Fischer, I. G. Savenko, M. Amthor, M. Lermer, A. Wolf, L. Worschech, V. D. Kulakovskii, I. A. Shelykh, M. Kamp, S. Reitzenstein, A. Forchel, Y. Yamamoto, and S. Höfling, An electrically pumped polariton laser, *Nature (London)* **497**, 348 (2013).
- [6] M. Z. Baten, P. Bhattacharya, T. Frost, S. Deshpande, A. Das, D. Lubyshev, J. M. Fastenau, and A. W. K. Liu, GaAs-based high

- temperature electrically pumped polariton laser, *Appl. Phys. Lett.* **104**, 231119 (2014).
- [7] J. Kasprzak, M. Richard, S. Kundermann, A. Baas, P. Jeambrun, J. M. J. Keeling, F. M. Marchetti, M. H. Szymańska, R. André, J. L. Staehli, V. Savona, P. B. Littlewood, B. Deveaud, and L. S. Dang, Bose-Einstein condensation of exciton polaritons, *Nature (London)* **443**, 409 (2006).
- [8] G. Malpuech, A. di Carlo, A. V. Kavokin, J. J. Baumberg, A. Zamfirescu, and P. Lugli, Room-temperature polariton lasers based on GaN microcavities, *Appl. Phys. Lett.* **81**, 412 (2002).
- [9] S. Christopoulos, G. Baldassarri Höger von Högersthal, A. J. D. Grundy, P. G. Lagoudakis, A. V. Kavokin, J. J. Baumberg, G. Christmann, R. Butté, E. Feltn, J.-F. Carlin, and N. Grandjean, Room-Temperature Polariton Lasing in Semiconductor Microcavities, *Phys. Rev. Lett.* **98**, 126405 (2007).
- [10] G. Christmann, R. Butté, E. Feltn, J.-F. Carlin, and N. Grandjean, Room temperature polariton lasing in a GaN/AlGaIn multiple quantum well microcavity, *Appl. Phys. Lett.* **93**, 051102 (2008).
- [11] A. Das, J. Heo, M. Jankowski, W. Guo, L. Zhang, H. Deng, and P. Bhattacharya, Room Temperature Ultralow Threshold GaN Nanowire Polariton Laser, *Phys. Rev. Lett.* **107**, 066405 (2011).
- [12] P. Bhattacharya, T. Frost, S. Deshpande, M. Z. Baten, A. Hazari, and A. Das, Room Temperature Electrically Injected Polariton Laser, *Phys. Rev. Lett.* **112**, 236802 (2014).
- [13] R. Jayaprakash, F. G. Kalaitzakis, G. Christmann, K. Tsagaraki, M. Hocevar, B. Gayral, E. Monroy, and N. T. Pelekanos, Ultra-low threshold polariton lasing at room temperature in a GaN membrane microcavity with a zero-dimensional trap, *Sci. Rep.* **7**, 5542 (2017).
- [14] K. Bejtka, F. Reveret, R. W. Martin, P. R. Edwards, A. Vasson, J. Leymarie, I. R. Sellers, J. Y. Duboz, M. Leroux, and F. Semond, Strong light-matter coupling in ultrathin double dielectric mirror GaN microcavities, *Appl. Phys. Lett.* **92**, 241105 (2008).
- [15] G. Christmann, D. Simeonov, R. Butté, E. Feltn, J.-F. Carlin, and N. Grandjean, Impact of disorder on high quality factor III-V nitride microcavities, *Appl. Phys. Lett.* **89**, 261101 (2006).
- [16] A. C. Tamboli, E. D. Haberer, R. Sharma, K. H. Lee, S. Nakamura, and E. L. Hu, Room-temperature continuous-wave lasing in GaN/InGaIn microdisks, *Nat. Photonics* **1**, 61 (2007).
- [17] A. C. Tamboli, M. C. Schmidt, S. Rajan, J. Speck, U. K. Mishra, Steven Denbaars, and E. L. Hu, Smooth top-down photoelectrochemical etching of *m*-plane GaN, *J. Electrochem. Soc.* **156**, H47 (2009).
- [18] E. Trichas, N. T. Pelekanos, E. Iliopoulos, E. Monroy, K. Tsagaraki, A. Kostopoulos, and P. G. Savvidis, Bragg polariton luminescence from a GaN membrane embedded in all dielectric microcavity, *Appl. Phys. Lett.* **98**, 221101 (2011).
- [19] K. S. Daskalakis, P. S. Eldridge, G. Christmann, E. Trichas, R. Murray, E. Iliopoulos, E. Monroy, N. T. Pelekanos, J. J. Baumberg, and P. G. Savvidis, All-dielectric GaN microcavity: Strong coupling and lasing at room temperature, *Appl. Phys. Lett.* **102**, 101113 (2013).
- [20] I. Aharonovich, A. Woolf, K. J. Russell, T. Zhu, N. Niu, M. J. Kappers, R. A. Oliver, and E. L. Hu, Low threshold, room-temperature microdisk lasers in the blue spectral range, *Appl. Phys. Lett.* **103**, 021112 (2013).
- [21] R. Jayaprakash, F. Kalaitzakis, M. Kayambaki, K. Tsagaraki, E. Monroy, and N. T. Pelekanos, Ultra-smooth GaN membranes by photo-electrochemical etching for photonic applications, *J. Mater. Sci.* **49**, 4018 (2014).
- [22] E. A. Amargianitakis, F. Miziou, M. Androulidaki, K. Tsagaraki, A. Kostopoulos, G. Konstantinidis, E. Delamadeleine, E. Monroy, and N. T. Pelekanos, Improved GaN quantum well microcavities for robust room temperature polaritonics, *Phys. Status Solidi B* **256**, 1800716 (2019).
- [23] O. Ambacher, J. Smart, J. R. Shealy, N. G. Weimann, K. Chu, M. Murphy, W. J. Schaff, L. F. Eastman, R. Dimitrov, L. Wittmer, M. Stutzmann, W. Rieger, and J. Hilsenbeck, Two-dimensional electron gases induced by spontaneous and piezoelectric polarization charges in N- and Ga-face Al-GaN/GaN heterostructures, *J. Appl. Phys.* **85**, 3222 (1999).
- [24] N. Grandjean, B. Damilano, S. Dalmaso, M. Leroux, M. Laügt, and J. Massies, Built-in electric-field effects in wurtzite Al-GaN/GaN quantum wells, *J. Appl. Phys.* **86**, 3714 (1999).
- [25] R. Langer, J. Simon, V. Ortiz, N. T. Pelekanos, A. Barski, R. André, and M. Godlewski, Giant electric fields in unstrained GaN single quantum wells, *Appl. Phys. Lett.* **74**, 3827 (1999).
- [26] J. Simon, R. Langer, A. Barski, and N. T. Pelekanos, Spontaneous polarization effects in GaN/AlGaIn quantum wells, *Phys. Rev. B* **61**, 7211 (2000).
- [27] V. Fiorentini, F. Bernardini, F. Della Sala, A. Di Carlo, and P. Lugli, Effects of macroscopic polarization in III-V nitride multiple quantum wells, *Phys. Rev. B* **60**, 8849 (1999).
- [28] E. Dimakis, A. Georgakilas, M. Androulidaki, K. Tsagaraki, G. Kittler, F. Kalaitzakis, D. Cengher, E. Bellet-Amalric, D. Jalabert, and N. T. Pelekanos, Plasma-assisted MBE growth of quaternary InAlGaIn quantum well heterostructures with room temperature luminescence, *J. Cryst. Growth* **251**, 476 (2003).
- [29] Kalaitzakis, M. Androulidaki, N. T. Pelekanos, E. Dimakis, E. Bellet-Amalric, D. Jalabert, D. Cengher, K. Tsagaraki, E. Aperathitis, G. Konstantinidis, and A. Georgakilas, Field-compensated quaternary InAlGaIn/GaN quantum wells, *Phys. Status Solidi B* **240**, 301 (2003).
- [30] P. Waltereit, O. Brandt, A. Trampert, H. T. Grahn, J. Menniger, M. Ramsteiner, M. Reiche, and K. H. Ploog, Nitride semiconductors free of electrostatic fields for efficient white light-emitting diodes, *Nature (London)* **406**, 865 (2000).
- [31] M. D. Craven, P. Waltereit, J. S. Speck, and S. P. DenBaars, Well-width dependence of photoluminescence emission from a-plane GaN/AlGaIn multiple quantum wells, *Appl. Phys. Lett.* **84**, 496 (2004).
- [32] T. J. Badcock, P. Dawson, M. J. Kappers, C. McAleese, J. L. Hollander, C. F. Johnston, D. V. Sridhara Rao, A. M. Sanchez, and C. J. Humphreys, Optical properties of GaN/AlGaIn quantum wells grown on nonpolar substrates, *Appl. Phys. Lett.* **93**, 101901 (2008).
- [33] M. A. Mastro, E. A. Imhoff, J. A. Freitas, J. K. Hite, and C. R. Eddy, Jr., Towards a polariton-based light emitter based on non-polar GaN quantum wells, *Solid State Comm.* **149**, 2039 (2009).
- [34] G. Rossbach, J. Levrat, A. Dussaigne, G. Cosendey, M. Glauser, M. Cobet, R. Butté, N. Grandjean, H. Teisseyre, M. Bockowski, I. Grzegory, and T. Suski, Tailoring the light-matter coupling in anisotropic microcavities: Redistribution of oscillator strength in strained *m*-plane GaN/AlGaIn quantum wells, *Phys. Rev. B* **84**, 115315 (2011).
- [35] J. Levrat, G. Rossbach, A. Dussaigne, G. Cosendey, M. Glauser, M. Cobet, R. I Butté, N. Grandjean, H. Teisseyre,

- M. Boćkowski, I. Grzegory, and T. Suski, Nonlinear emission properties of an optically anisotropic GaN-based microcavity, *Phys. Rev. B* **86**, 165321 (2012).
- [36] R. Tao, M. Arita, S. Kako, K. Kamide, and Y. Arakawa, Strong coupling in non-polar GaN/AlGaIn microcavities with air-gap/III-nitride distributed Bragg reflectors, *Appl. Phys. Lett.* **107**, 101102 (2015).
- [37] R. Tao, K. Kamide, M. Arita, S. Kako, and Y. Arakawa, Room-temperature observation of trapped exciton-polariton emission in GaN/AlGaIn microcavities with air-gap/III-nitride distributed Bragg reflectors, *ACS Photonics* **3**, 1182 (2016).
- [38] C. B. Lim, A. Ajay, and E. Monroy, Gallium kinetics on m-plane GaN, *Appl. Phys. Lett.* **111**, 022101 (2017).
- [39] C. B. Lim, A. Ajay, C. Bougerol, B. Haas, J. Schörmann, M. Beeler, J. Lähnemann, M. Eickhoff, and E. Monroy, Nonpolar m-plane GaN/AlGaIn heterostructures with intersubband transitions in the 5–10 THz band, *Nanotechnology* **26**, 435201 (2015).
- [40] Q. S. Paduano, D. W. Weyburne, and D. H. Tomich, Growth and properties of m-plane GaN on m-plane sapphire by metalorganic chemical vapor deposition, *J. Cryst. Growth* **367**, 104 (2013).
- [41] T. Kawashima, T. Nagai, D. Iida, A. Miura, Y. Okadome, Y. Tsuchiya, M. Iwaya, S. Kamiyama, H. Amano, and I. Akasaki, Epitaxial lateral growth of m-plane GaN and Al_{0.18}Ga_{0.82}N on m-plane 4H-SiC and 6H-SiC substrates, *J. Cryst. Growth* **298**, 261 (2007).
- [42] A. Kobayashi, S. Kawano, Y. Kawaguchi, J. Ohta, and H. Fujioka, Room temperature epitaxial growth of m-plane GaN on lattice-matched ZnO substrates, *Appl. Phys. Lett.* **90**, 041908 (2007).
- [43] A. Das, S. Magalhães, Y. Kotsar, P. K. Kandaswamy, B. Gayral, K. Lorenz, E. Alves, P. Ruterana, and E. Monroy, Indium kinetics during the plasma-assisted molecular beam epitaxy of semipolar (11–22) InGaIn layers, *Appl. Phys. Lett.* **96**, 181907 (2010).
- [44] See Supplemental Material at <http://link.aps.org/supplemental/10.1103/PhysRevB.104.125311> for experimental measurements on GaN/AlGaIn quantum well exciton states and further details on GaN-based membranes.
- [45] P. Misra, U. Behn, O. Brandt, H. T. Grahn, B. Imer, S. Nakamura, S. P. DenBaars, and J. S. Speck, Polarization anisotropy in GaN films for different nonpolar orientations studied by polarized photoreflectance spectroscopy, *Appl. Phys. Lett.* **88**, 161920 (2006).
- [46] R. Kucharski, M. Rudziński, M. Zając, R. Doradziński, J. Garczyński, L. Sierżputowski, R. Kudrawiec, J. Serafińczuk, W. Strupiński, and R. Dwiliński, Nonpolar GaN substrates grown by ammonothermal method, *Appl. Phys. Lett.* **95**, 131119 (2009).
- [47] P. Misra, O. Brandt, H. T. Grahn, H. Teisseyre, M. Siekacz, C. Skierbiszewski, and B. Lucznik, Complete in-plane polarization anisotropy of the A exciton in unstrained A-plane GaN films, *Appl. Phys. Lett.* **91**, 141903 (2007).
- [48] H. T. Grahn, Nonpolar-oriented GaN films for polarization-sensitive and narrow-band photodetectors, *MRS Bull.* **34**, 341 (2009).
- [49] P. Corfdir, A. Dussaigne, H. Teisseyre, T. Suski, I. Grzegory, P. Lefebvre, E. Giraud, J.-D. Ganière, N. Grandjean, and B. Deveaud-Plédran, Thermal carrier emission and nonradiative recombinations in nonpolar (Al,Ga)N/GaN quantum wells grown on bulk GaN, *J. Appl. Phys.* **111**, 033517 (2012).
- [50] B. Rau, O. Brandt P. Waltereit, M. Ramsteiner, K. H. Ploog, J. Puls, and F. Henneberger, In-plane polarization anisotropy of the spontaneous emission of M-plane GaN/(Al,Ga)N quantum wells, *Appl. Phys. Lett.* **77**, 3343 (2000).
- [51] E. A. Amargianitakis, R. Jayaprakash, F. G. Kalaitzakis, E. Delamadeleine, E. Monroy, and N. T. Pelekanos, Absorption in ultrathin GaN-based membranes: the role of standing wave effects, *J. Appl. Phys.* **126**, 083109 (2019).
- [52] S. Ghosh, P. Waltereit, O. Brandt, H. T. Grahn, and K. H. Ploog, Polarization-dependent spectroscopic study of M-plane GaN on γ -LiAlO₂, *Appl. Phys. Lett.* **80**, 413 (2002).
- [53] S. Shokhovets, L. Kirste, J. H. Leach, S. Krischok, and M. Himmerlich, Anisotropic optical constants, birefringence, and dichroism of wurtzite GaN between 0.6 eV and 6 eV, *J. Appl. Phys.* **122**, 045706 (2017).
- [54] E. A. Amargianitakis, S. A. Kazazis, G. Doundoulakis, G. Stavrinidis, G. Konstantinidis, E. Delamadeleine, E. Monroy, and N. T. Pelekanos, Transferrable dielectric DBR membranes for versatile GaN-based polariton and VCSEL technology, *Microelectron. Eng.* **228**, 111276 (2020).
- [55] S. A. Furman and A. V. Tikhonravov, *Basics of Optics of Multilayer Systems*, 1–102 (Editions Frontières, Gif-sur Yvette, 1992).
- [56] F. Tassone and Y. Yamamoto, Exciton-exciton scattering dynamics in a semiconductor microcavity and stimulated scattering into polaritons, *Phys. Rev. B* **59**, 10830 (1999).
- [57] C. Ciuti, P. Schwendimann, B. Deveaud, and A. Quattropani, Theory of the angle-resonant polariton amplifier, *Phys. Rev. B* **62**, R4825 (2000).
- [58] G. Rossbach, J. Levrat, G. Jacopin, M. Shahmohammadi, J.-F. Carlin, J.-D. Ganière, R. Butté, B. Deveaud, and N. Grandjean, High-temperature Mott transition in wide-band-gap semiconductor quantum wells, *Phys. Rev. B* **90**, 201308(R) (2014).
- [59] J. Kasprzak, R. André, L. S. Dang, I. A. Shelykh, A. V. Kavokin, Y. G. Rubo, K. V. Kavokin, and G. Malpuech, Build up and pinning of linear polarization in the Bose condensates of exciton polaritons, *Phys. Rev. B* **75**, 045326 (2007).
- [60] R. Butté, J. Levrat, G. Christmann, E. Feltn, J.-F. Carlin, and N. Grandjean, Phase diagram of a polariton laser from cryogenic to room temperature, *Phys. Rev. B* **80**, 233301 (2009).